remote sensing

MDPI

Article

The Change Pattern and Its Dominant Driving Factors of Wetlands in the Yellow River Delta Based on Sentinel-2 Images

Cuixia Wei [1], Bing Guo [1,2,3,4,5,*], Yewen Fan [6], Wenqian Zang [5] and Jianwan Ji [7]

1 School of Civil Architectural Engineering, Shandong University of Technology, Zibo 255000, China
2 State Key Laboratory of Resources and Environmental Information System, Institute of Geographic Sciences and Natural Resources Research of Chinese Academy of Sciences, Beijing 100101, China
3 Key Laboratory of Urban Land Resources Monitoring and Simulation, Ministry of Natural Resources, Shenzhen 518000, China
4 Key Laboratory of National Geographic Census and Monitoring, Ministry of Natural Resources, Wuhan 430072, China
5 Aerospace Information Research Institute, Chinese Academy of Sciences, Beijing 100101, China
6 State Key Laboratory of Information Engineering in Surveying, Mapping and Remote Sensing, Wuhan University, Wuhan 430079, China
7 School of Geography Science and Geomatics Engineering, Suzhou University of Science and Technology, Suzhou 215009, China
* Correspondence: guobing@sdut.edu.cn

Abstract: There were significant differences in the dominant driving factors of the change process of different types of wetlands in the Yellow River delta. In addition, to our knowledge, the optimal classification feature sets with the Random Forest algorithm for wetlands in the Yellow River delta were least explored. In this paper, the wetland information in the study area was extracted based on a Random Forest algorithm with de-feature variable redundancy, and then the change process of wetland and its dominant factors from 2015 to 2021 was monitored and analyzed using the Geodetector and gravity center model. The results showed that (1) the optimal variable sets composed of red edge indexes based on the Random Forest algorithm had the highest classification accuracy, with the overall accuracy and Kappa coefficient of 95.75% and 0.93. (2) During 2015–2021, a large area of natural wetland in the Yellow River delta was transformed into an artificial wetland. The wetlands showed an overall development direction of "northwest–southeast" along the Yellow River. (3) The interaction between vegetation coverage and accumulated temperature had the largest explanatory power of the change in the natural wetland area. The interaction between solar radiation and DEM had the largest explanatory power for the change in the artificial wetland area. The research results could better provide decisions for wetland protection and restoration in the Yellow River delta.

Keywords: wetlands; change pattern; Random Forest algorithm; feature selection; Geodetector

check for updates

Citation: Wei, C.; Guo, B.; Fan, Y.; Zang, W.; Ji, J. The Change Pattern and Its Dominant Driving Factors of Wetlands in the Yellow River Delta Based on Sentinel-2 Images. *Remote Sens.* **2022**, *14*, 4388. https://doi.org/10.3390/rs14174388

Received: 6 August 2022
Accepted: 1 September 2022
Published: 3 September 2022

Publisher's Note: MDPI stays neutral with regard to jurisdictional claims in published maps and institutional affiliations.

Copyright: © 2022 by the authors. Licensee MDPI, Basel, Switzerland. This article is an open access article distributed under the terms and conditions of the Creative Commons Attribution (CC BY) license (https://creativecommons.org/licenses/by/4.0/).

1. Introduction

Wetlands, an important ecosystem, can provide critical functions and values in water supply, biodiversity maintenance, climate regulation, and water purification. Under the double stress of global climate change and intensified human activity, the wetlands showed a degradation trend, with the shrink area and declined function. Effective monitoring of wetland change processes can help reveal and understand the causes of degradation, which is conducive to better restoring ecological functions and promoting wetland ecological health. Therefore, monitoring the change patterns of wetlands and determining their dominant driving factors are essential for regional sustainable development [1]. The Yellow River delta (YRD) refers to the alluvial plain formed by the sediments carried by the Yellow River in the depression of the Bohai Sea, which has the most complete temperate wetland ecosystem in China. It was officially listed as an important international wetland in 2013. At present, the YRD faces three serious ecological challenges: the severe formalization of

wetland protection, the low degree of wetland development and utilization, and the decline of ecological service functions. The ecological conservation and high-quality development of the Yellow River Basin is a major national strategy. Strengthening wetland protection and ecological governance in the lower reaches of the Yellow River is one of the keys to ensuring the implementation of this strategy. Therefore, it is very important to reveal the evolutionary characteristics, laws, and patterns of wetland ecosystems in the YRD.

In recent years, remote sensing has become an effective tool for monitoring the condition and change process of wetlands. Traditional classification methods include unsupervised classification [2] and rule-based classification supported by GIS [3]. When extracting and classifying wetland information with multispectral data, the maximum likelihood classification algorithm was the most commonly used method, but this method could only provide 30–60% classification accuracy [4]. Later, scholars found that Classification and Regression Tree (CART) [5], Support Vector Machine (SVM) [6], and Artificial Neural Network (ANN) [7] could improve the classification accuracy of wetlands. Khatami et al. [8] proved through experiments that the pixel-based classification algorithms in the past 15 years, which showed that the classification accuracy of SVM and Random Forest (RF) algorithms were the highest, followed by an ANN, and the maximum likelihood classification was a commonly used benchmark algorithm with low classification accuracy. Noi and Kappas [9] examined and compared the performances of the RF, KNN (K-Nearest Neighbors), and SVM classifiers for land use/cover classification using Sentinel-2 image data, and all three classifiers showed similar and high overall accuracy. Dehkordi et al. [10] proposed a new clustering method that used the Function of the Mask to generate a training sample for supervised monitoring of long-term water surface dynamics. Gxokwe et al. [11] assessed the capabilities of GEE (Google Earth Engine) cloud-computing platform in characterizing small seasonal flooded wetlands, which showed RF, SVM, and CART had superiority. When using the methods above to extract and classify wetland information, the key to intelligent wetland information classification is the extraction and optimization of multiple feature variables of remote sensing images. The primary feature variables used in wetland information extraction and classification are spectral features and their derivative factors, texture features, temporal features, and DEM (Digital Elevation Model) [12,13]. However, classification accuracy and efficiency were greatly affected by many feature variables. Therefore, it was crucial to optimize the feature variables according to local conditions before classification. In recent years, it has been found that the RF algorithm has great advantages in the determination of the optimal subset of feature variables, and it can automatically judge the importance of variables and give dependence among variables [14]. It provided a novel approach to determining the optimal feature variables for wetland classification for our study [15].

In recent years, many scholars have studied the evolutionary patterns of wetlands in the YRD. Wang et al. [16] investigated wetland degradation and analyzed its causation. Liu et al. [17] quantified the spatial and temporal dynamics of wetlands in the YRD from the class and landscape levels. Moreover, Zhou [18] used the low-medium resolution Landsat data to simulate the evolution trend of wetland in YRD and found that there was a reduced area of 954.03 km^2 for wetland in 1976–2016, and the constructed wetland was spreading into the sea. However, the dominant factors of different types of wetland changes in the YRD during different historical periods are currently unclear.

At present, the RF algorithm has been used in many studies on wetland information extraction and classification. However, these studies were conducted without considering the advantages of the RF algorithm that could remove the redundancy of feature variables. Feature optimization was of great importance in wetland information extraction and classification [19]. In addition, the wetland ecosystem of the YRD has undergone dramatic changes due to the combined impacts of climate change and human activities. However, the spatio-temporal change patterns of wetlands and their dominant driving factors in different periods are unclear. The objectives of this paper are as follows: (1) to determine the optimal feature variable sets for wetlands classification in the YRD; (2) to extract the

information of wetlands in the YRD based on the RF algorithm and the optimal feature variable sets; (3) to monitor and reveal the change patterns of the wetland ecosystem and its driving mechanisms in the YRD based on the Geodetector and gravity center model, which provided the basis for the protection and rational utilization of wetland resources in the YRD [20].

2. Materials and Methods

2.1. Study Area

The Yellow River delta, located in the Yellow River estuary of Dongying City, Shandong Province, China (117°31′–119°18′E, 36°55′–38°16′N), has the youngest and most complete wetland ecosystem, with an area of approximately 7033.405 km^2 (Figure 1). In this study region, a large area of mud flats and wetlands is formed under river–sea integration actions. The soil types in the study area are mainly composed of coastal saline soil and tidal soil. The terrain is flat, with an average altitude less than 15 m. It belongs to a temperate monsoon climate with distinct seasons and sufficient light. Since the 1980s, a decrease in sediments in the Yellow River Basin has led to serious seawater recharge and coastal erosion, which is conducive to the formation of salinization.

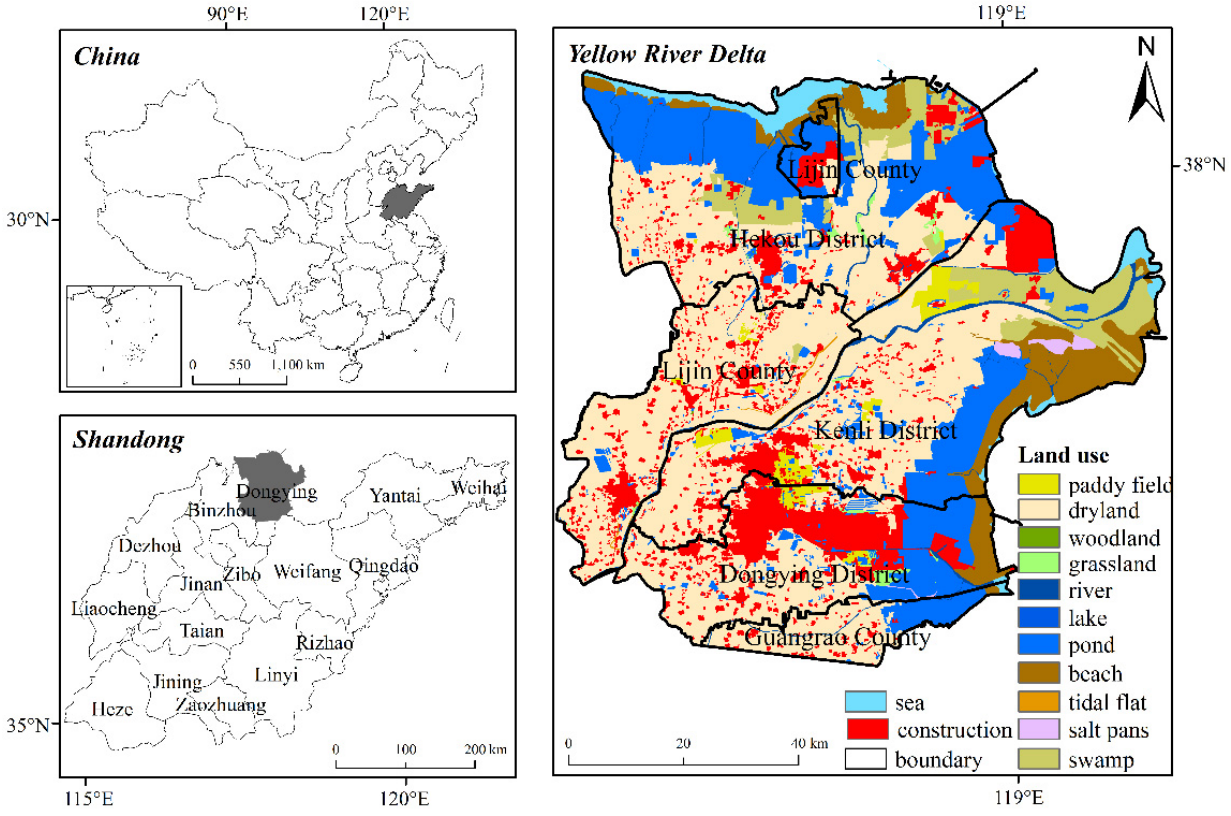

Figure 1. Location of the study area.

2.2. Data Source and Preprocessing

To achieve the accurate extraction of wetland information in the YRD, this study selected a Sentinel-2 remote sensing image with a higher spatial resolution (10 m) and more available bands (13 bands) (United States Geological Survey, https://earthexplorer.usgs.gov/, accessed on 13 September 2015 and 8 September 2021) in August and September as the data source. The hydrological characteristics of the YRD in August and September were relatively stable in the growing seasons, which could better distinguish different vegetation types. The red-edge index derived from the red-edge bands of Sentinel-2 images had a large contribution rate in the process of extracting and classifying wetland information in the YRD [21]. The Sen2cor atmospheric correction model of SNAP software was used to elimi-

nate the noises of atmospheric and aerosols. In addition, ENVI 5.5 was applied to conduct the process of BRDF (Bidirectional Reflectance Distribution Function) correction [22]. The final datasets after atmospheric correction and BRDF correction were at a spatial resolution of 10 m. The driving factors, including vegetation coverage (FVC), precipitation, soil type, and Gross Domestic Product (GDP), were obtained from the Resource and Environmental Science and Data Centre (https://www.resdc.cn/, accessed on 15 September 2021).

2.3. Methods

In this paper, the overall technical flowchart is shown in Figure 2.

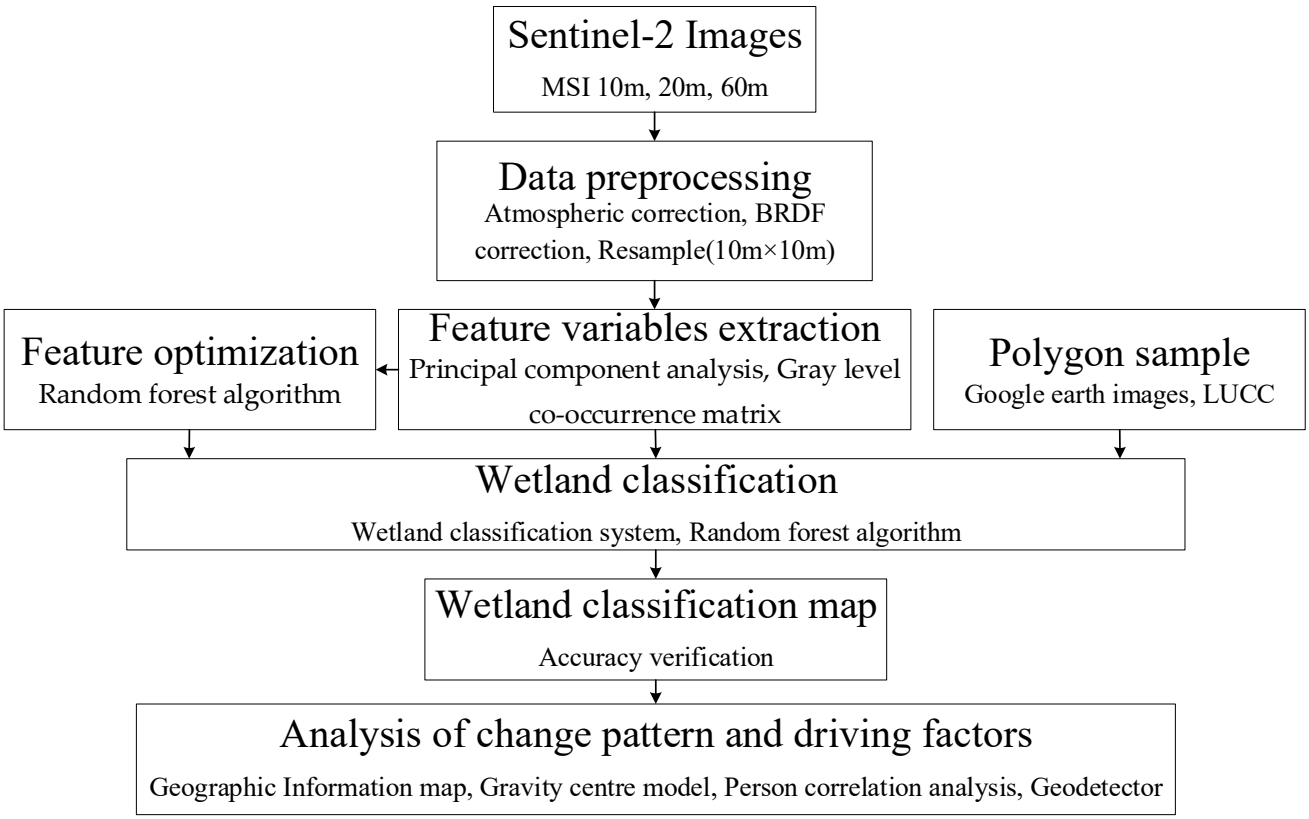

Figure 2. Overall technical flowchart of this study.

2.3.1. Classification System of Wetlands

Wetlands were composed of natural or artificial, permanent, or temporary swamps, wet sources, mire lands or water areas, water bodies with static or flowing fresh, brackish, or salt water, and waters with a depth of not more than 6 m at low tide [23]. Combined with the actual situation of the YRD, the wetland classification system (Table 1) in this paper was formulated based on the national wetland classification standard. To accurately extract wetland information in the YRD, this study described the geometric and image features of ground objects based on Sentinel-2 images and high-resolution Google Earth images.

Table 1. Classification system of wetlands in the YRD.

First Classification	Secondary Classification	Remote Sensing Image	Geometric Feature
Natural wetland	River		Green or yellow, slender striped.
	Swamp		Dark green, irregular shape, largely distributed in nature reserves.
	Mud flat		Yellow, striped, distributed in coastal areas.
	Shallow sea		Green, striped, distributed in coastal areas.
Artificial wetland	Salt pans		Green or gray-white, grid-like, coastal distribution.
	Paddy field		Bright green, striped, distributed along the river.
	Reservoirs pond	 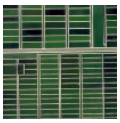	Reservoir pond: Green, regular in shape, scattered in the study area; Loose pond: Green, striped, distributed in coastal areas.
Non-wetland	Dryland		Green, regular shape, with evident texture features.
	Woodland		Dark green, distributed along roads and rivers.
	Construction land		Pink and gray hybrid, regular in shape, distributed inland.
	Unused land	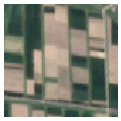	Soil yellow, scattered distribution.

2.3.2. Description of Feature Variables

Based on Sentinel-2 images, this study extracted 35 feature variables, including spectral feature, texture feature [24–26], vegetation index, water index, red-edge index, and others [27], which are shown in Table 2.

Table 2. Descriptions of the feature variables derived from Sentinel-2 images.

Feature Variable Set	Index Full Name	Index [28,29]	Characteristic Description	Resolution (m)
Spectral feature	Band	B	B_2, B_3, B_4, B_5, B_6, B_7, B_8, B_{8A}, B_{11}, B_{12}	10
Texture feature	ASM	GLCM_ASM	–	10
	Contrast	GLCM_Con	–	10
	Dissimilarity	GLCM_Dis	–	10
	Energy	GLCM_Ene	–	10
	Entropy	GLCM_Ent	–	10
	Homogeneity	GLCM_Hom	–	10
	MAX	GLCM_MAX	–	10
	GLCM_Correlation	GLCM_Cor	–	10
	GLCM_Mean	GLCM_Mean	–	10
	GLCM_Variance	GLCM_Var	–	10
Vegetation index	Normalized Difference Vegetation Index	NDVI	$(B_{8a} - B_4)/(B_{8a}+B_4)$	10
	Ratio Vegetation Index	RVI	B_{8a}/B_4	10
	Difference Vegetation Index	DVI	$B_{8a} - B_4$	10
	Modified Soil Adjusted Vegetation Index	MSAVI	$\frac{(2B_{8a}+1)-\sqrt{(2B_{8a}+1)^2-8(B_{8a}-B_4)}}{2}$	10
	Soil Adjusted Vegetation Index	SAVI	$1.5(B_{8a} - B_4)/(B_{8a}+B_4+0.5)$	10
Water index	Normalized Difference Water Index	NDWI	$(B_3 - B_{8a})/(B_3+B_{8a})$	10
	Modified Normalized Difference Water Index	MNDWI	$(B_3 - B_{11})/(B_3+B_{11})$	10
Red-edge index	Red-edge Normalized Difference Vegetation Index	RNDVI	$(B_5 - B_4)/(B_5+B_4)$	10
	Chlorophyll Index red-edge	CIre	B_{8a}/B_5-1	10
	Modified Simple Ratio Index red-edge	MSRre	$\frac{B_7/B_4-1}{\sqrt{B_7/B_4+1}}$	10
	Normalized Difference Vegetation Index red-edge1	NDVIre1	$(B_{8a} - B_5)/(B_{8a}+B_5)$	10
	Normalized Difference Vegetation Index red-edge2	NDVIre2	$(B_{8a} - B_6)/(B_{8a}+B_6)$	10
	Normalized Difference Vegetation Index red-edge3	NDVIre3	$(B_{8a} - B_7)/(B_{8a}+B_7)$	10
	Normalized Difference red-edge1	NDre1	$(B_6 - B_5)/(B_6+B_5)$	10
	Normalized Difference red-edge2	NDre2	$(B_7 - B_5)/(B_7+B_5)$	10

B_2 is the blue band, B_3 is the green band, B_4 is the red band, B_5 is the vegetation red edge1 band, B_6 is the vegetation red edge2 band, B_7 is the vegetation red edge3 band, B_8 is near-infrared band, B_{8a} is narrow near-infrared band, B_{11} is short-wave infrared1 band, B_{12} is short-wave infrared2 band.

2.3.3. Texture Information Extraction

(1) Principal component analysis

Principal component analysis (PCA) is a dimension reduction mathematical statistical method [30]. With the help of the orthogonal transformation, the component-related original random variables were transformed into new component-independent random

variables, named the principal component [31,32]. In this paper, PCA was applied to eliminate the mutual influences among the bands of Sentinel-2 images, reduce the workload of texture information extraction, and improve work efficiency with the tools of spatial analyst of ArcGIS 10.5.

(2) Gray level co-occurrence matrix

A gray level co-occurrence matrix (GLCM) can be used to extract the texture information of Sentinel-2 images, which was proposed by Haralick in 1973 [33]. First, the GLCM of the image was calculated, and then second-order statistical characteristics describing the texture were obtained based on this matrix, which has strong adaptability and robustness [34,35]. GLCM has been widely used in the texture extraction of SAR, multispectral, high-resolution images. Texture is a degree-dependent phenomenon caused by the interaction of the hue primitive space of an image [36]. The equation is as follows:

$$P_{i,j}(d,Q) = \begin{array}{c} \#\{(x_1,y_1)(x_2,y_2)|f(x_1,y_1) = \\ i, f(x_2,y_2) = j, |(x_1,y_1) - (x_2,y_2)| = \\ d, L((x_1,y_1),(x_2,y_2)) = \theta\} \end{array} \quad (1)$$

where, # is the number of elements in the dataset; $f(x_1,y_1) = i$ represents the pixel gray of image position (x_1,y_1); d represents the distance between two pixels, θ represents the direction angle between two pixels; d ranges from 1 to 4; θ refers to the values of 0°, 45°, 90°, and 135°.

2.3.4. Random Forest Algorithm

The random forest algorithm plays an important role in feature selection and dimension reduction, and is an algorithm for generating multiple decision trees through ensemble learning based on the CART algorithm invented by Breiman et al. [37,38]. It allows the fusion of high-dimensional data from multiple sources and has a strong tolerance for missing values and outliers. It is suitable for dealing with high-dimensional complex datasets and can automatically determine the importance of feature variables.

A classification accuracy model sequence a is obtained by K-round training, which forms a multi-classification model system $\{h_1(X), h_2(X), \ldots, h_k(X)\}$. The final classification result can be obtained by a simple majority voting decision. The final classification decision was as follows:

$$H(x) = \arg\max \sum_{i=1}^{K} I(h_i(x) = Y) \quad (2)$$

where $H(x)$ represents the combination classification model, $h_i(x)$ represents a single decision tree classification model, Y represents an output variable, $I(h_i(x) = Y)$ is the representation function [39].

2.3.5. Confusion Matrix

The confusion matrix is also called the error matrix, which has been widely used to compare the degree of confusion between classification results and actual measured values. This study applied the overall accuracy (OA), Kappa coefficient (Kappa), producer's accuracy (PA), and user's accuracy (UA) to evaluate the accuracy of each classification [40].

$$\mathrm{OA} = \frac{\sum_{i=1}^{k} N_{ii}}{N} \quad (3)$$

$$\mathrm{Kappa} = \frac{N\sum_{i=1}^{k} N_{ii} - \sum_{i=1}^{k} N_{i+}N_{+i}}{N^2 - \sum_{i=1}^{k} N_{i+}N_{+i}} \quad (4)$$

$$\mathrm{PA}_i = \frac{N_{ii}}{N_{+i}} \quad (5)$$

$$\mathrm{UA}_i = \frac{N_{ii}}{N_{i+}} \quad (6)$$

where N is the total number of samples, k is the total number of categories, N_{ii} is the number of samples correctly classified, N_{i+} and N_{+i} are the number of actual samples and predicted samples of the i-th category, respectively.

3. Results

3.1. Wetland Information Extraction and Classification

3.1.1. Feature Optimization

In the classification process, there is a certain information redundancy among the 35 feature variables, which can increase the calculation complexity and reduce the accuracy in the process of classification. Therefore, it is necessary to optimize the feature variables before classification. The RF algorithm can not only be used to realize the classification of wetlands but also play an important role in feature selection and dimensional reduction. In this paper, the out-of-bag (OOB) data error of RF was used to calculate the importance of the feature variables and to determine the optimal feature variables. The expression of the importance of feature variables $V\left(X^j\right)$ was as follows:

$$V\left(X^j\right) = \frac{1}{N}\sum_{t=1}^{n}\left(e_t^j - e_t\right) \quad (7)$$

where, n is the number of decision trees in random forests, e_t is the OOB error of each decision tree calculated by OOB, X^j is the random assignment of the *j-th* feature variable of the OOB data, e_t^j is the OOB error calculated by the new value X^j. The change of variable X^j leads to an increase in OOB error and a decrease in accuracy.

According to the formula above, the importance score of 35 feature variables in the YRD in 2021 was calculated and is then shown in Figure 3. The GLCM_Variance ranked first, with an importance score of 0.1317, followed by the MNDWI, with an importance score of 0.1084. The importance scores of NDWI and GLCM_Mean were the same at 0.1046. The texture features for Homogeneity and Dissimilarity had smaller importance scores of 0.005 and 0.0005, respectively. According to the comprehensive feature set, the contribution rate of feature variables in the classification process of wetland in the YRD was ranked as red-edge index > vegetation and water index > spectral feature > texture feature. The contribution rate of the red-edge index was about 37.5%, while that of vegetation and water index was 25%. The contribution rates of spectral features and texture features were smaller at 20% and 17.5%, respectively.

The correlation matrix of the 35 feature variables in 2021 is shown in Figure 4. GLCM_variance was extremely strongly correlated with B11, the correlation coefficient was 0.84, and the correlation coefficient of MNDWI with B11 was 0.83; therefore, B11 should be removed [41]. The correlation coefficient thresholds are shown in Table 3. Similar to this process, 15 feature variables were removed. Finally, 20 feature variables were selected to construct the optimal feature variable sets for the classification of wetlands based on Sentinel-2 images. Compared to 2021, there was a certain degree of change in the types and spatial distribution patterns of wetlands in 2015, which led to the fluctuation of the importance scores of feature variables. Depending on the selection principles, the optimal feature variable sets for wetlands classification of the YRD in 2015 and 2021 are obtained in Table 4. There were slight differences in the feature variables between 2015 and 2021. However, the contribution rates of the feature variable set had the same ranking, which showed that the red-edge index had the greatest contribution rate in the process of wetland information extraction and classification.

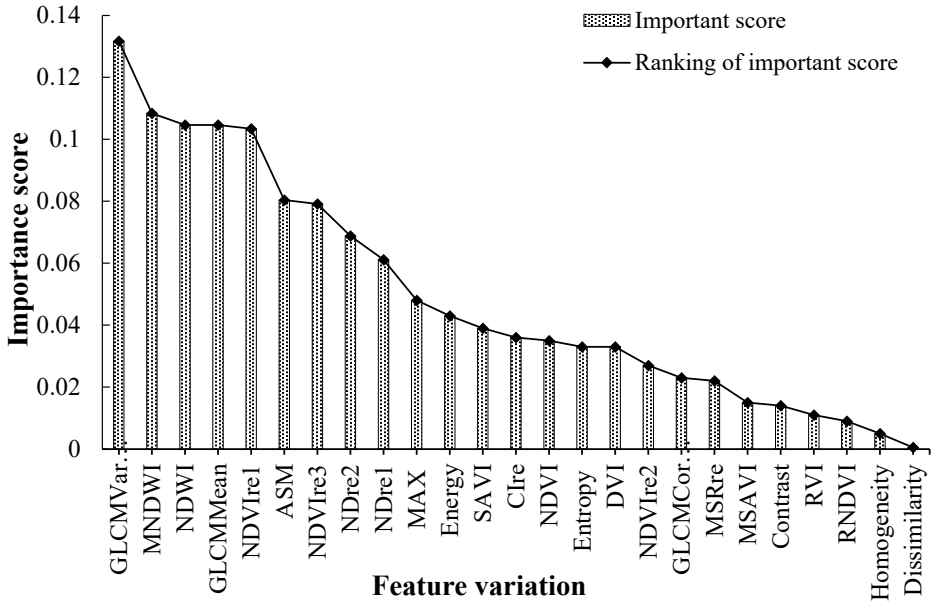

Figure 3. The importance scores and rankings of different feature variables in 2021.

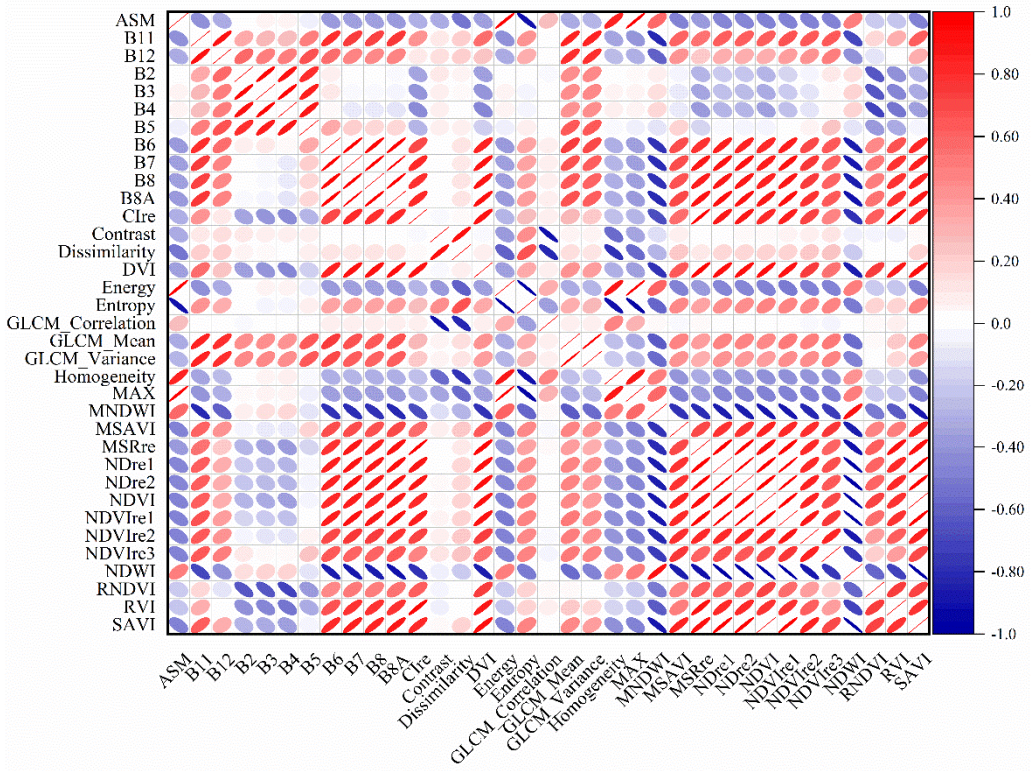

Figure 4. Correlation matrix among 35 feature variables in 2021.

Table 3. Correlation levels of the correlation coefficient.

Correlation	Extremely Strong Correlation	Strong Correlation	Moderate Correlation	Low Correlation	Uncorrelation
correlation coefficient	>0.8 <−0.8	0.6~0.8 −0.8~−0.6	0.4~0.6 −0.6~−0.4	0.2~0.4 −0.4~−0.2	<0.2 >−0.2

Table 4. The optimal feature variable sets for 2015 and 2021.

Year	The Optimal Combination of Features
2015	B2, B3, B4, B5, GLCM_Variance, RNDVI, GLCM_Mean, MNDWI, MSAVI, RVI, Energy, DVI, MSRre, NDVIre1, NDVIre3, NDre1, NDre2, Cire, NDVI, NDVIre2
2021	B2, B3, B4, B5, GLCM_Variance, ASM, Energy, GLCM_Correlation, MNDWI, MSAVI, NDVIre1, NDVIre3, NDre1, NDre2, Cire, NDVI, NDVIre2, RNDVI, RVI, DVI

3.1.2. Construction of the Classification Scheme

As shown in Table 5, six classification schemes were designed in this paper. Scheme A only used the spectral features of Sentinel-2 images (except B1, B9, B10). Scheme B was composed of spectral features, vegetation index, and water index. Scheme C was used to select the spectral features of the Sentinel-2 images and the red-edge index. Scheme D was composed of spectral and texture features, while scheme E was a combination of all feature variables. Scheme F was composed of the optimal feature variable sets determined by the RF algorithm. The main purposes of setting different classification schemes are: (1) To investigate the contribution rate of different feature variables to wetland information extraction and determine the importance ranking of different feature variables; (2) To explore the optimal method to improve the extraction and classification of wetland information by comparing the accuracy among different classification schemes.

Table 5. Descriptions of the classification scheme.

Classification Scheme	Feature Combination
A	Spectral feature
B	Spectral feature + Vegetation index + Water index
C	Spectral feature+ Red-edge index
D	Spectral feature + Texture feature
E	Spectral feature + Vegetation index + Water index + Red-edge index + Texture feature
F	The optimal feature variables set

3.1.3. Accuracy Evaluation Analysis

It can be seen from Table 6 that the OA and Kappa of scheme A based on the spectral features were 82.91% and 0.82, respectively. After adding the vegetation index, water index, and red-edge index to scheme A, the classification accuracy of schemes B and C was slightly improved, with OA of 83.87% and 84.21%, and Kappa of 0.83 and 0.82, respectively. However, the classification accuracy of scheme D with texture features and scheme F with all feature variables decreased, with the OA of 81.74% and 81.54% and Kappa values of 0.80 and 0.79, respectively. This indicated that the vegetation index, water index, and red-edge index could improve the accuracy of wetland information extraction and classification, but the texture features derived from Sentinel-2 images with a spatial resolution of 10 m were not conducive to improving the accuracy of wetland information extraction. The OA and Kappa of classification scheme F were enhanced to 95.75% and 0.93, respectively, indicating that classification scheme F had the best applicability for wetland classification in the YRD.

Table 6. Statistics for classification accuracy.

Land Cover Type	A		B		C		D		E		F	
	PA %	UA %	PA %	UA %	PA %	UA %	PA %	UA %	PA %	UA %	PA %	UA %
River	63.98	83.74	62.73	82.11	63.35	79.69	50	67.82	59.32	81.4	79.37	82.05
Swamp	62.50	64.52	59.38	66.67	70.31	75.00	79.79	72.82	64.71	70.21	95.45	96.78
Mud flat	94.39	91.82	96.26	95.37	93.46	93.46	94.03	99.21	97.01	93.53	99.77	99.64
Shallow sea	86.59	87.65	87.80	83.72	91.46	87.21	94.66	88.57	92.37	95.53	92.91	98.58
Salt pans	94.12	87.50	94.96	87.60	93.70	90.28	87.08	84.89	88.19	86.59	67.08	56.34
Paddy field	92.21	87.12	93.51	89.44	93.51	88.89	84.91	85.71	89.62	93.14	95.24	100
Reservoirs and pond	84.15	77.00	83.61	78.06	85.25	77.23	84.77	78.04	86.8	76.34	99.5	97.88
Dryland	81.31	76.99	81.31	79.82	82.24	81.48	66.93	75.22	70.87	69.23	91.15	96.55
Woodland	65.57	83.33	75.41	83.64	77.05	88.68	81	77.88	64	72.73	74.74	71.14
Construction land	92.42	84.72	90.15	85.00	92.42	87.77	86.72	81.62	84.38	77.7	95.24	92.25
Unused land	78.12	94.34	79.69	85.00	87.50	91.80	72.55	74	66.67	79.07	98.29	95.82
OA	83.81		84.26		85.89		81.74		81.54		95.75	
Kappa	0.81		0.83		0.84		0.80		0.79		0.93	

Single type of PA and UA could show that vegetation index and the red-edge index were conductive to improve the accuracy of wetland information classification. In schemes B and C, the accuracy of swamp, paddy field, and dryland were enhanced after adding the above two feature sets, and the contribution rate of the red-edge index was higher than that of the vegetation index. Texture features improved the accuracy of mud flat, shallow sea, reservoirs, ponds, and construction land, which indicated that the texture features could contribute to the classification of objects with evident texture information. When all the feature variables were involved in the classification, classification accuracy and Kappa were reduced due to information redundancy. In classification scheme F, the feature variables with high correlation were removed, which avoided the interference of overlapping redundant information on wetland information extraction and classification. The classification results are shown in Figure 5.

3.1.4. Wetland Information Extraction and Classification Results

Utilizing the optimal feature variable sets and RF algorithm, the spatial distribution of wetlands in 2015 and 2021 was obtained. As shown in Figure 6a, in 2015, the area of the natural wetland was 986.99 km^2, while that of the artificial wetland was 1334.33 km^2. In the natural wetland, the mud flat had the largest area of 432.90 km^2, accounting for 6.16 % of the total area, which was mainly distributed in the northern Hekou district, the coastal area of Kenli district, and eastern Dongying district. The shallow sea had the second largest area of 353.47 km^2, accounting for 5.03% of the total area, which was mostly located in the northern Hekou district, coastal areas in the Kenli district, and eastern Dongying district. The area of swamp was 129.79 km^2, accounting for 1.85 %, which was mostly distributed in the estuary of the Yellow River in the northeast of Kenli district. The river had the smallest area of 70.82 km^2, accounting for only 1.01% of the total area. In the artificial wetland, the reservoirs and pond had the largest area of 926.30 km^2, accounting for 13.19%, followed by salt pans, with an area of 274.66 km^2, accounting for 3.91%, which was mainly distributed in the northern Hekou district, Kenli district, Dongying district, and eastern Guangrao county. The paddy field area was 133.37 km^2, accounting for only 1.90% of the total area, which was largely distributed in the central and northeastern Kenli district.

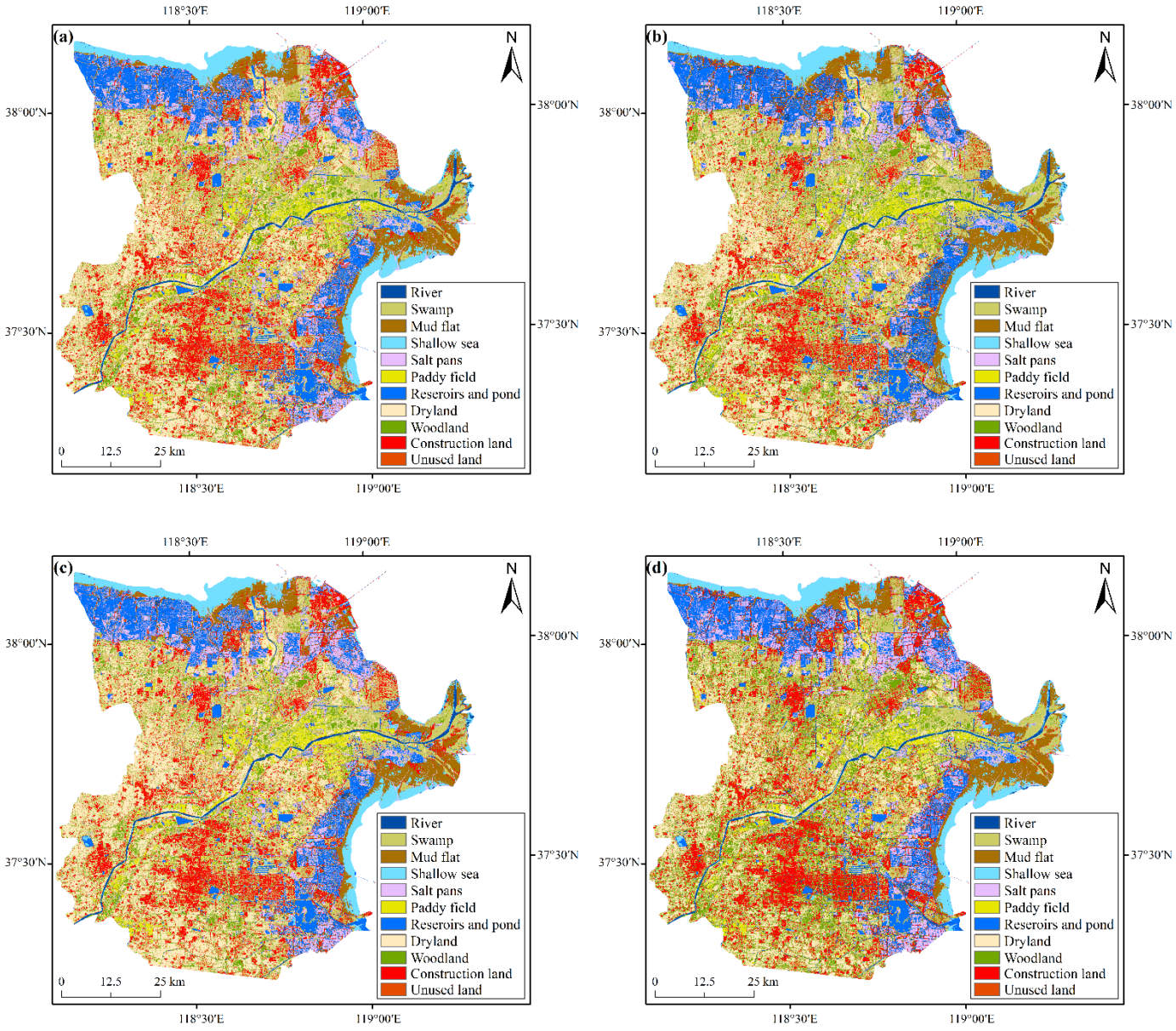

Figure 5. *Cont.*

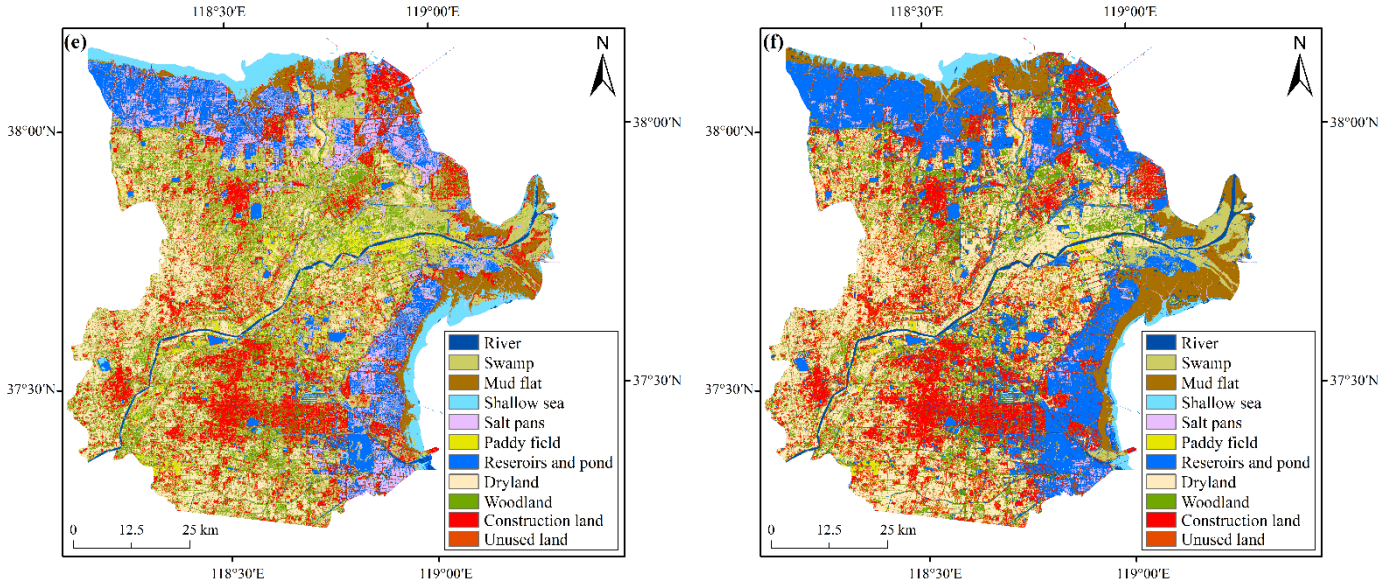

Figure 5. The spatial distributions of wetlands in 2021: (**a**) spectral feature; (**b**) spectral feature + vegetation index + water index; (**c**) spectral feature + red-edge index; (**d**) spectral feature + texture feature; (**e**) all features; (**f**) the optimal feature variable sets.

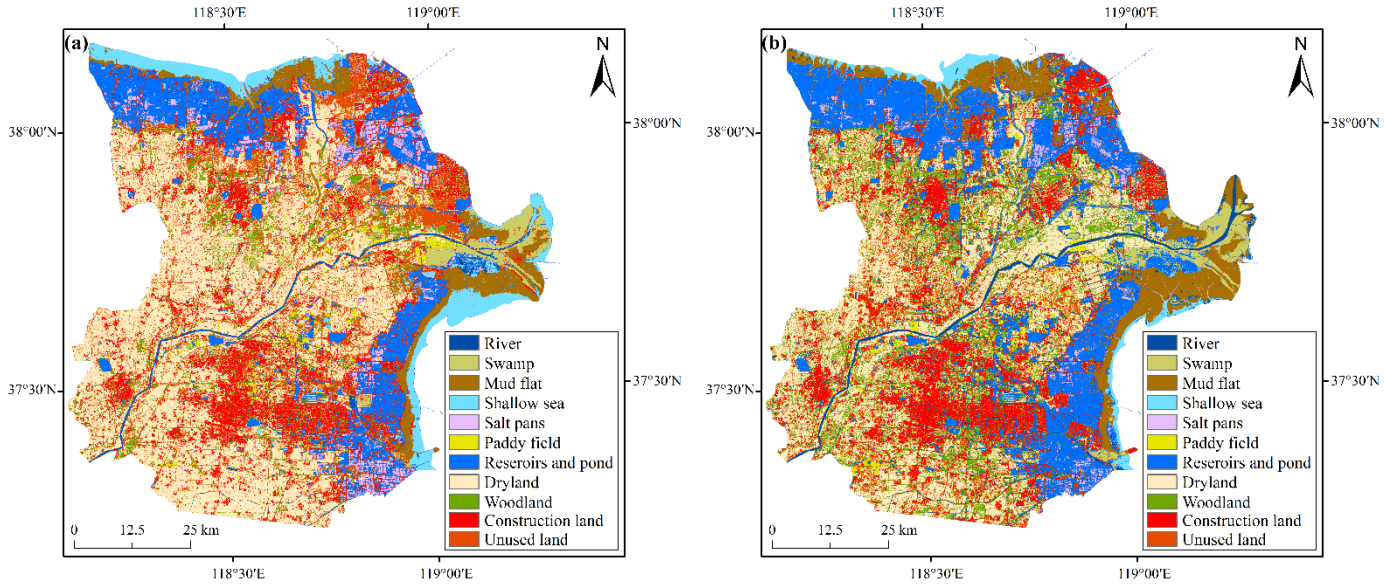

Figure 6. Spatial distribution of wetlands in the YRD: (**a**) 2015; (**b**) 2021.

As shown in Figure 6b, in 2021, the area of the natural wetland was 1239.93 km^2, while that of the artificial wetland was 1573.22 km^2. In the natural wetland, the mud flat had the largest area of 658.23 km^2, accounting for 9.36% of the total area, which was mostly distributed in the northern Hekou district, the coastal area of Kenli district, and the eastern Dongying district. The river had the second largest area of 290.97 km^2, accounting for 4.14%, which was composed of the Yellow River and the Guangli River. The area of swamp was 155.18 km^2, accounting for 2.21%, which was mostly distributed in the northeast of the YRD Nature Reserve in the Kenli district. The shallow sea had the smallest area of 135.55 km^2, accounting for only 1.93%, which was mostly distributed along the coastline. In the artificial wetland, reservoirs, and ponds had the largest area of 1286.21 km^2, accounting for 18.29% of the total area. The salt pans had the second largest area of 151.22 km^2, accounting for 2.15% of the total area, which was mostly distributed in coastal areas. The

paddy field had the smallest area of 135.79 km^2, accounting for only 1.93% of the total area, which was mainly distributed in the rivers and lakes of the Kenli district.

3.2. Change Patterns of Wetland during 2015–2021 in YRD

3.2.1. Spatial Distribution of Wetland Changes

The change patterns of the primary classification of wetlands in the YRD during 2015–2021 are shown in Figure 7. The YRD had the largest area of land cover as unchanged (5871.75 km^2), followed by that of the new-born area, with an area of 674.82333 km^2. The internal conversion area of wetland occupied 288.98 km^2 and the extinction group had the smallest area of 239.59 km^2. The extinction area of wetlands had the smallest area of 239.59 km^2. Among them, the unchanged area, internal conversion area, and extinction area covered the largest area in the Kenli district with 1826.29 km^2, 118.33 km^2 and 83.12 km^2, respectively. In the Hekou district, the unchanged area, internal conversion area, and extinction area covered an area of 1769.66 km^2, 97.90 km^2 and 65.46 km^2, respectively. However, the new-born wetland had the largest area of 242.69 km^2. In Guangrao county, the unchanged area, the internal conversion area, extinction area, and new-born area covered the smallest area of 276.83 km^2, 11.44 km^2, 5.09 km^2 and 23.70 km^2. Table 7 is the comparison table of wetland change types in Figure 7.

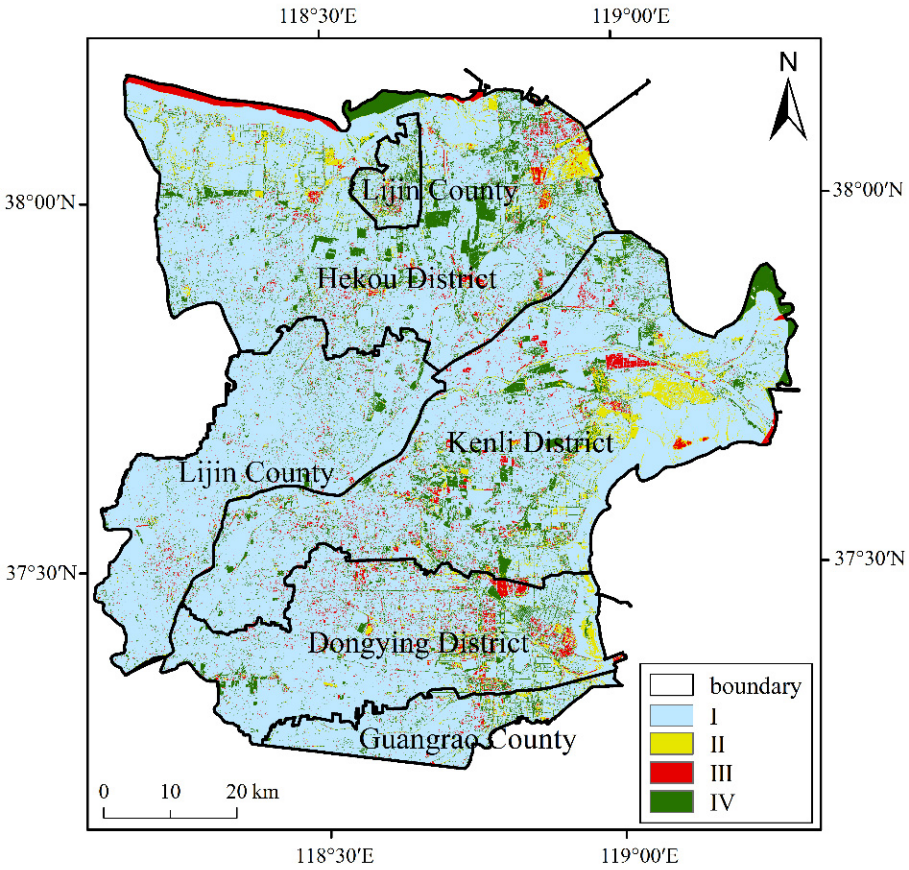

Figure 7. Spatial distribution of primary classification changes in land cover. I Unchanged area; II Internal conversion area; III Extinction area; IV New-born area.

Table 7. Comparison of primary classification change patterns.

Number	Type	Meaning
I	Unchanged area	Land cover did not change
II	Internal conversion area	Conversion between natural/constructed wetlands
III	Extinction area	Conversion of natural/constructed wetlands to non-wetlands
IV	New-born area	Conversion of non-wetlands to natural/constructed wetlands

The change patterns of the secondary classification of wetlands during 2015–2021 are shown in Figure 8. The zone of unclassified land converted to reservoirs and ponds had the largest area of 142.29 km^2. The zone of salt pans converted to reservoirs and ponds had the second largest area of 139.79 km^2. The conversion area from shallow sea to mud flat covered an area of 129.89 km^2, while that of the conversion area from mud flat to shallow sea was only 1.79 km^2. For the internal conversion area of wetland, the zone of salt pans converted to reservoirs and ponds in the Hekou district had the largest area of 70.62 km^2, accounting for 50.52 % of this conversion-type area, followed by that of the Kenli district, with an area of 28.41 km^2, accounting for 20.32% of this conversion-type area. The zone of shallow sea converted to mud flat in the Kenli district had the largest area of 68.94 km^2, accounting for 53.08% of this conversion-type area, followed by that of the Hekou district, with an area of 54.48 km^2, accounting for 41.94%. In the extinction area of wetland, the zone of mud flat converted to construction land in the Dongying district had the largest area of 55.80 km^2, accounting for 34.91%, followed by that of the Hekou district, accounting for 30.87%. The swamp zone converted to dryland in the Kenli district had the second largest area of 43.32 km^2, accounting for the largest proportion of 61.56%. In the new-born wetland area, the zone of unused land converted to reservoirs and ponds had the largest area, while that of the Hekou district and Kenli district accounted for 46.13% and 28.85%, respectively. The dryland zone converted to paddy field had the second largest area of 87.00 km^2, while that of Kenli district and Lijin county accounted for 41.46% and 23.66 %, respectively. Secondary classification coding of land cover and wetland types in the YRD is shown in Table 8.

As shown in Figure 9a,b, the area of the new-born paddy field that derived from dryland was 111.63 km^2, accounting for 77.93%. The extinction area of the paddy field was 88.31 km^2, of which 49.06% converted to dryland. The area of the new-born shallow sea was 26.99 km^2, while that of the extinction area of the shallow sea was 51.87 km^2. The areas of new-born salt pans and reservoirs and ponds were 22.35 km^2 and 316.27 km^2, and the conversion area percentages from unused land were 41.13% and 44.99%, respectively. The areas of extinction salt pans and reservoirs and reservoirs and ponds were 18.69 km^2 and 42.63 km^2, which mostly changed into construction land, with conversion ratios of 51.35% and 59.60%, respectively. As shown in Figure 9c, 50.45% of paddy fields, 77.55% of salt pans, 82.35% of rivers, 47.97% of mud flats, and 46.14 % of swamps were converted to reservoirs and ponds, and 62.97% of shallow seas were converted to mud flats.

Table 8. The secondary classification coding of land cover and wetland types in the YRD.

Number	01	02	03	04	05	06
Land cover	Paddy field	Shallow sea	Salt pans	Reservoirs and pond	Dryland	Woodland
Number	07	08	09	10	11	12
Land cover	River	Mud flat	Construction land	Swamp	Unused land	Sea

Notes: The first two digits and the last two digits represent the land cover types shown in Table 8, and the third digit 0 represents the conversion process. For example, 01001 represents the unchanged area of paddy fields, and 01003 represents paddy fields converted to salt pan areas.

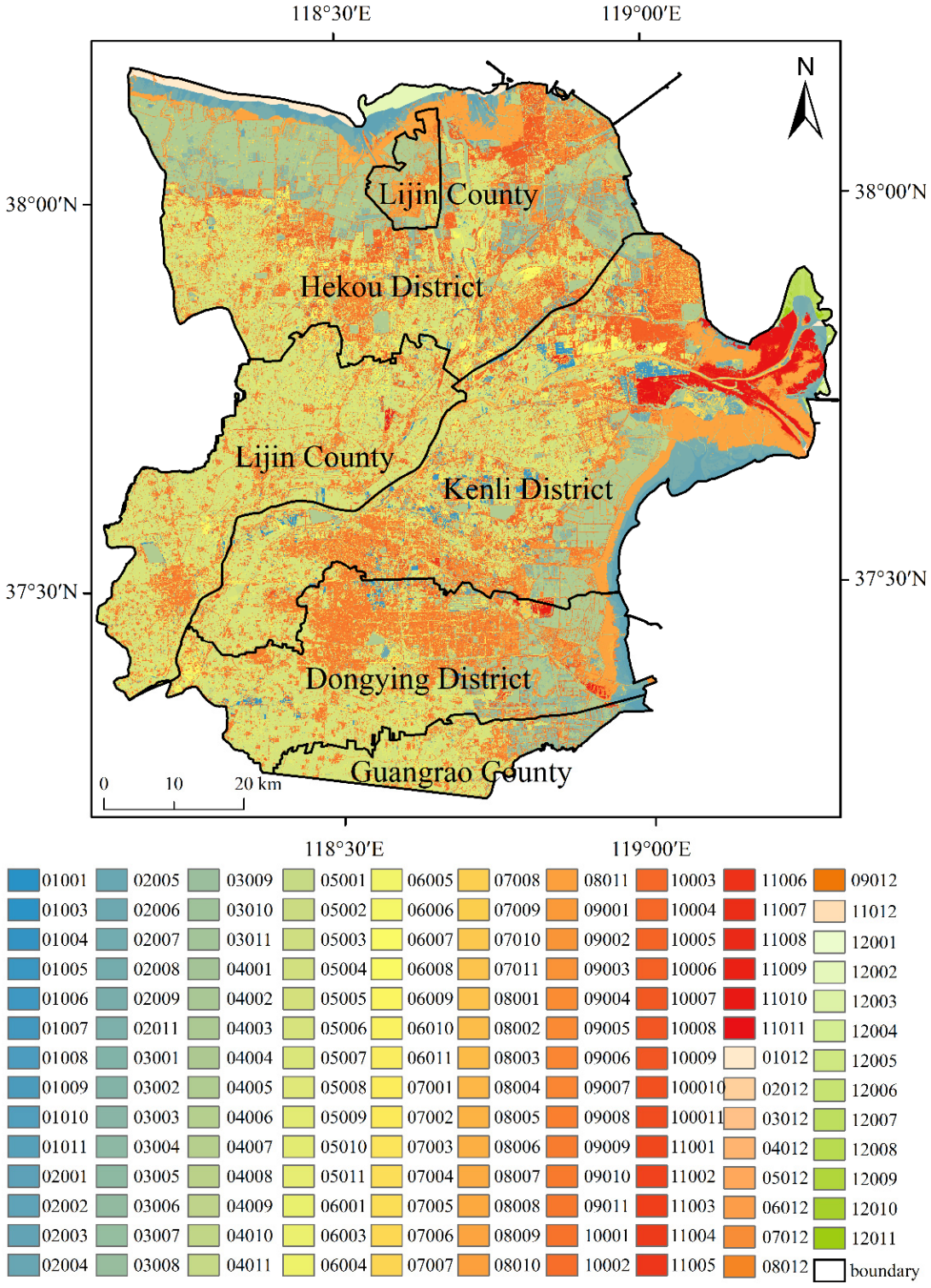

Figure 8. Spatial distributions of secondary classification changes during 2015–2021.

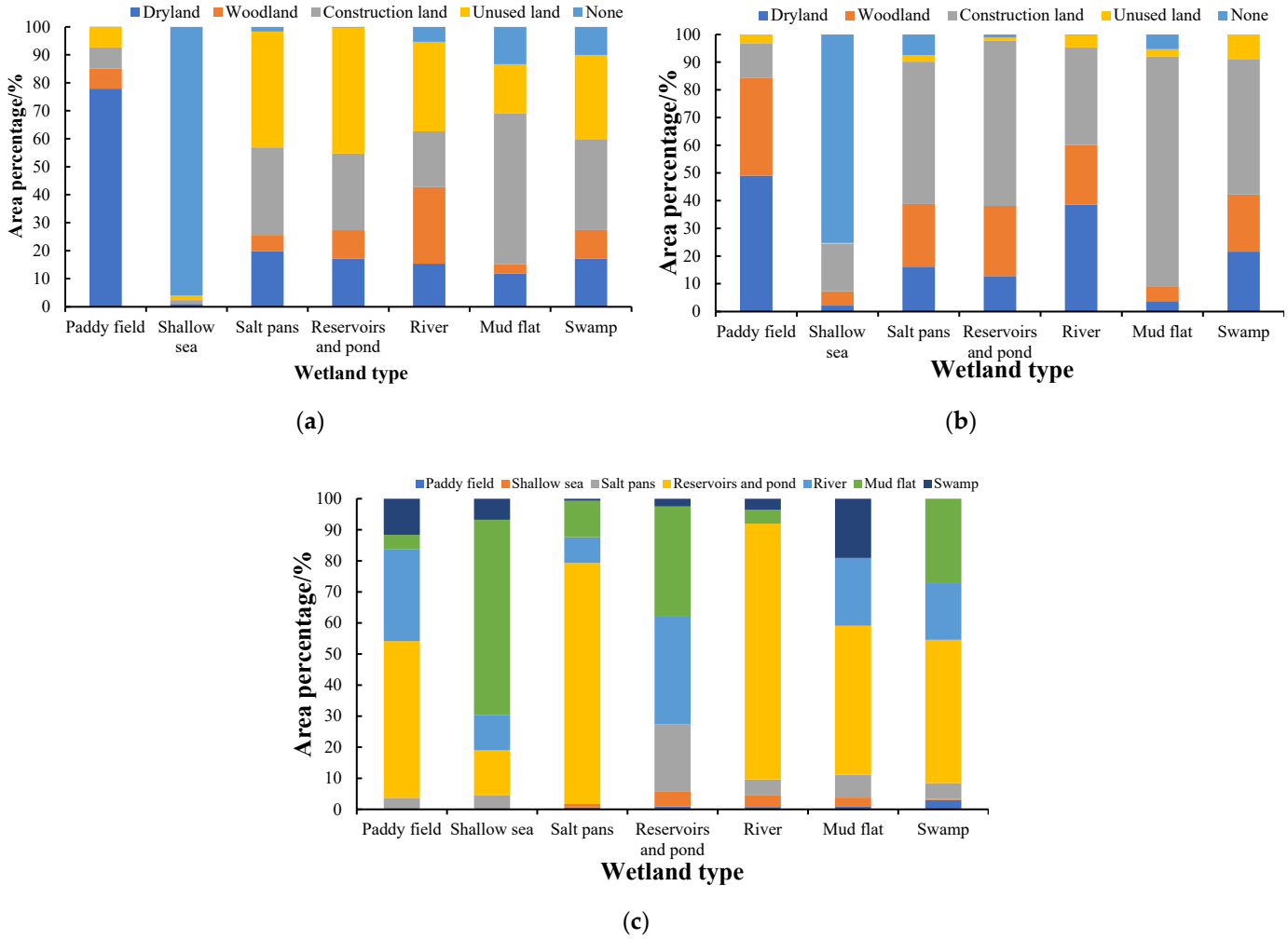

Figure 9. Area proportion of different wetland types. (**a**) Area proportion of sources for new-born wetlands; (**b**) Area proportion of land uses for extinction wetlands; (**c**) Area proportion of internal conversion among wetlands.

3.2.2. Gravity Center Migrations for Different Wetlands

The migration trajectory of the gravity center for wetlands could reflect the spatial heterogeneity and bias of the change patterns of different wetland types in varying periods [42–44]. As shown in Figure 10, the gravity center of each wetland type in the YRD was distributed along the Yellow River Basin from 2015 to 2021. Among them, the gravity center of the paddy field migrated from northeast to southwest, while that of the shallow sea and river moved from southeast to northwest. The gravity center of reservoirs and pond migrated from northwest to southeast, while that of mud flat moved from south to north. The long half axis of the standard deviation ellipse was significantly larger than the short half axis, indicating that the change direction of the wetlands in the YRD was more remarkable from 2015 to 2021. The increasing trend of wetlands in the southwest and northeast was significantly greater than that in the other directions. The migration directions of gravity centers of different wetland types in the YRD from 2015 to 2021 are shown in Table 9.

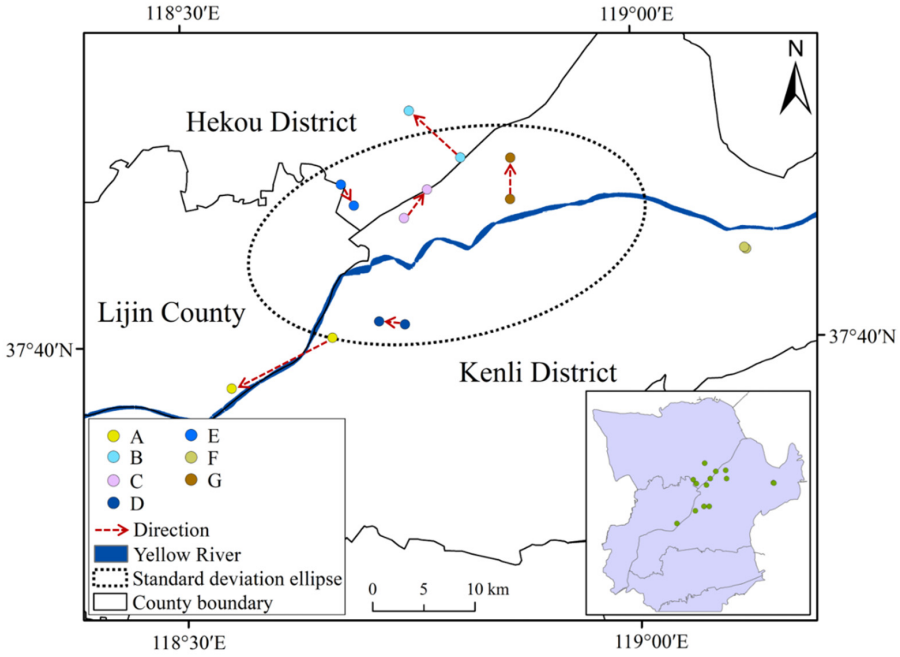

Figure 10. Migration directions of gravity centers of different wetland types in the YRD from 2015 to 2021.

Table 9. Type codes for wetlands.

Number	A	B	C	D	E	F	G
Type of wetland	puddy field	shallow sea	salt pans	river	reservoirs and pond	swamp	mud flat

3.3. Dominant Driving Factors of Wetland Changes during 2015–2021

3.3.1. Single Factor

The spatial distribution of various wetlands in the YRD was affected by both natural and human factors. Correlation analysis was applied to measure the correlations between two or more associated variables [45,46]. Based on the method for the simple linear regression analysis, the correlation between the wetland area and the mean value of influencing factors was analyzed under the confidential level of 95%. The correlation coefficient R is shown in Table 10.

Table 10. The correlation levels of r.

Correlation	High Correlation	Moderate Correlation	Mild Correlation	Low Correlation	Uncorrelation
r	>0.95 <−0.95	0.8~0.95 −0.95~−0.8	0.5~0.8 −0.8~−0.5	0.3~0.5 −0.5~−0.3	<0.3 >−0.3

As shown in Figure 11a, there was high correlation between wetland area and FVC, with r = −0.961. The primary reason was that zones with higher FVC were mostly dominated by dryland and woodland, which were mainly distributed in the northwest of Kenli district on both sides of the Yellow River Basin and inland, the southern part of Hekou district, Lijin county, Dongying district, and the western part of Guangrao county. The wetland was mostly distributed in the northern part of Hekou district, Kenli district, and the eastern part of Dongying district. The wetlands were mainly composed of Suaeda salsa, which is a typical salt-accumulating halophyte with lower vegetation coverage. As shown in Figure 11b, the correlation between wetland area and precipitation was moderate,

with r = 0.850. The wetland area increased with the increase in precipitation. The primary reason was that more precipitation would increase soil moisture content and river runoff supply, and promote the expansion of wetland area. As shown in Figure 11c, the correlation between wetland area and coastal saline soil area was high, with r = 0.960. The reason was that aquaculture reservoirs, ponds, and salt pans were mainly concentrated in coastal areas with severe salinization. As shown in Figure 11d, there was a moderate correlation between wetland area and GDP, with r = 0.847. The primary reason was that, since 2009, economic development has been beneficial to the rational development and utilization of wetland resources, which would protect wetland resources.

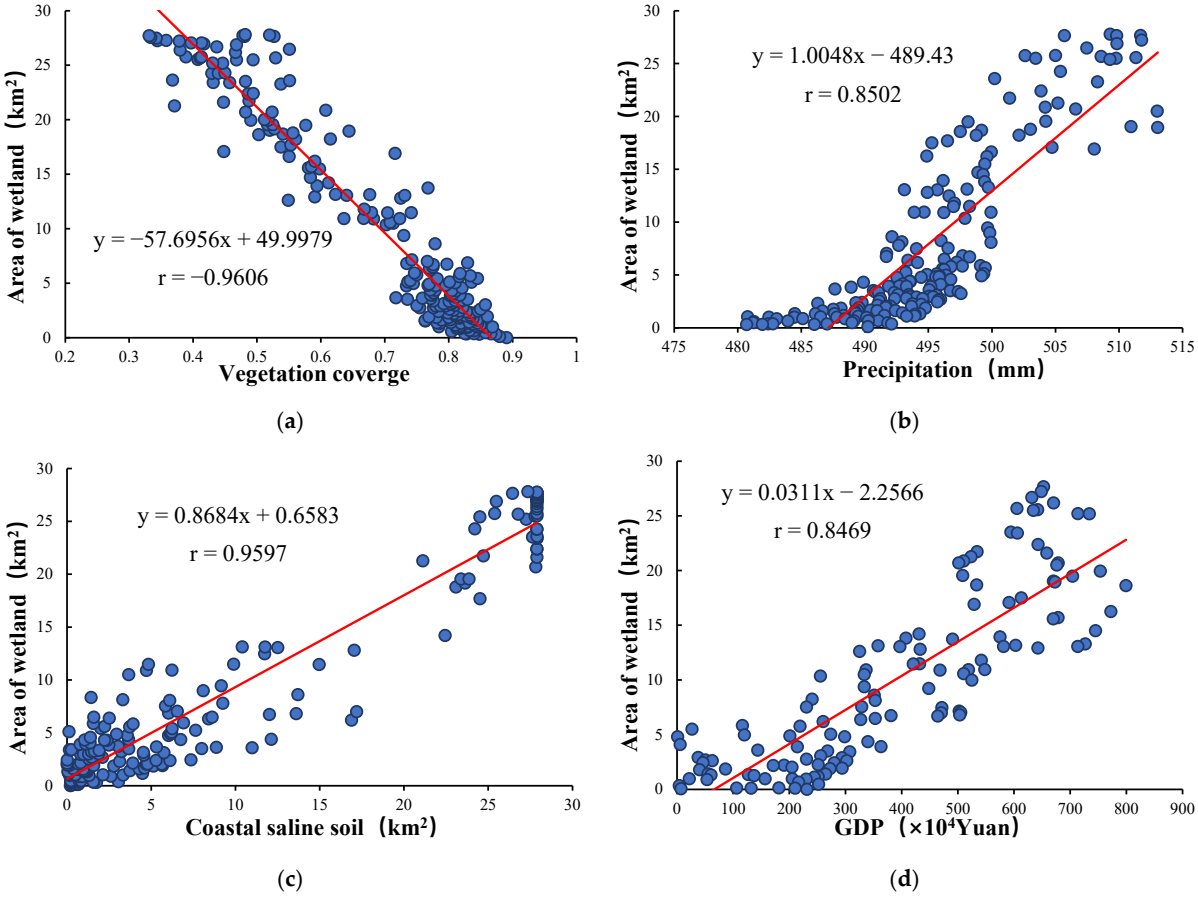

Figure 11. Correlation between wetland area and driving factors. (**a**) Vegetation coverage; (**b**) Precipitation; (**c**) Coastal saline soil area; (**d**) GDP.

3.3.2. Interaction Factors

The combined impacts (Figure 12c, d) of the change of wetlands in YRD had a higher q-value than individual impacts (Figure 12a, b) on the change of wetlands. Approximately 36 pairwise combinations with three different types of interactions were formed between the 9 driving factors. Most drivers exhibited non-linear enhancement when interacting with the change of wetlands, followed by bi-factor enhancement unique-variable weakening interactions. As shown in Figure 12c, solar radiation, when interacting with accumulated temperature, showed bi-factor enhancement and explained 86.3% of the change in the natural wetland. Bi-factor enhancement occurred when the combined influence (solar radiation + accumulated temperature = 1.253) of the two variables was greater than individual (solar radiation = 0.448 and accumulated temperature = 0.805) and interaction influences (solar radiation and accumulated temperature = 0.863) on the response variable. Nonlinear enhancement occurred when the interaction influence (FVC and temperature = 0.797) was greater than that of the individual (FVC=0.098 and temperature=0.648) and com-

bined (FVC + temperature = 0.746) variables. Unique variable weakening occurred when individual variable (precipitation = 0.531) influence was greater than either combined (precipitation + slope = 0.594) or interaction (precipitation + slope = 0.512) effects on a response variable [47].

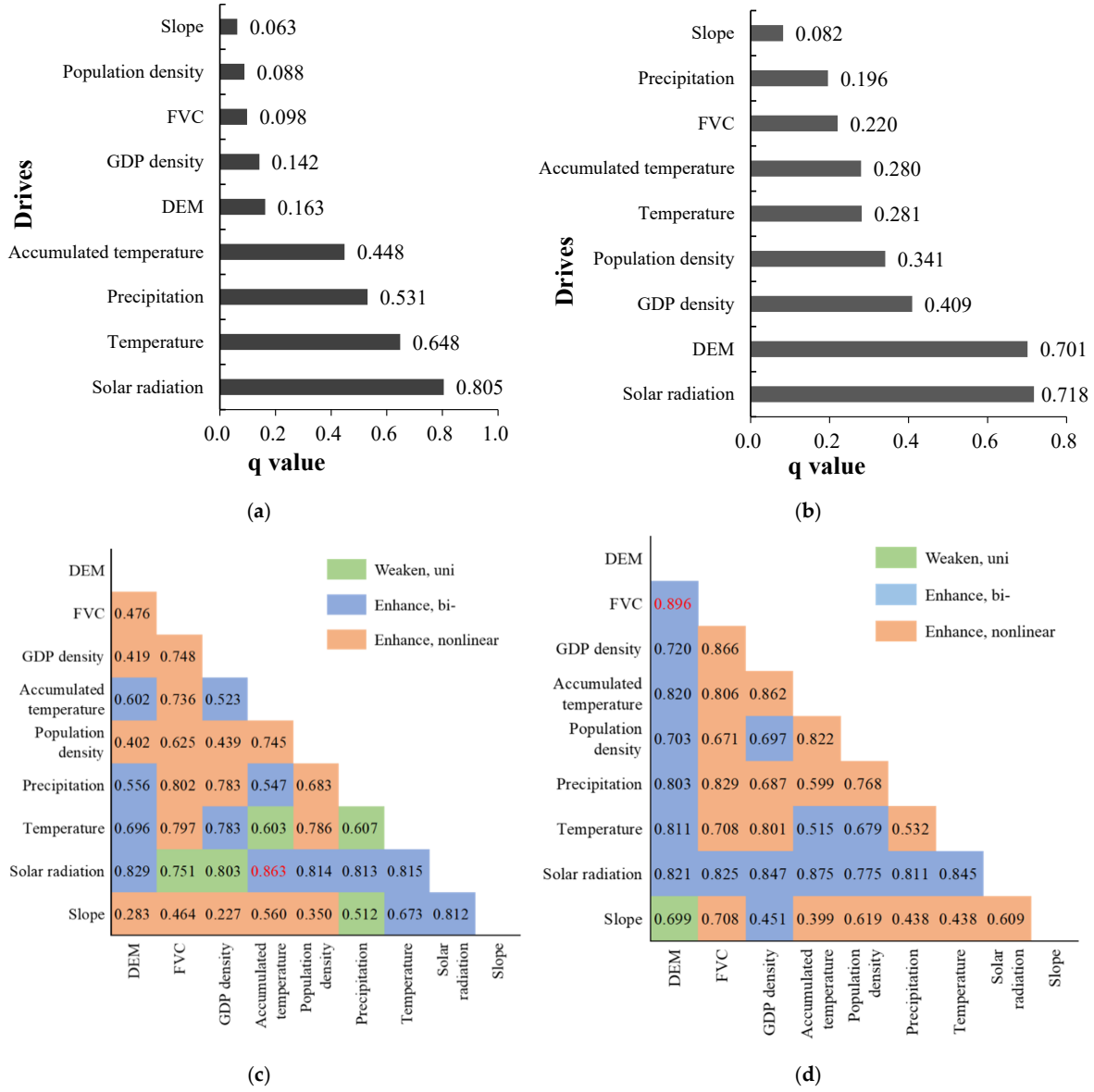

Figure 12. The dominant factors of the change in wetlands. (**a**) Natural wetland; (**b**) Artificial wetland. The dominant interaction factors of the change in wetlands. (**c**) Natural wetlands; (**d**) Artificial wetlands.

As shown in Figure 12d, FVC interaction with DEM and accumulated temperature caused bi-factor enhancement and explained 89.6% and 82.0% of the change in artificial wetlands, respectively. Socioeconomic variable interactions, such as GDP density and population density, explained 69.7% of the change in artificial wetlands. Climate and socioeconomic variable interactions, such as GDP density and accumulated temperature, population density, and precipitation, explained 86.2% and 76.8% of the change in artificial wetland, respectively. On the other hand, DEM showed non-linear enhancement when interacting with slope because of their weak individual influence on the change of artificial wetlands.

It can be seen that solar radiation and accumulated temperature had larger explanatory power on the change of natural wetlands, while FVC and DEM contributed greatly to the changes of artificial wetlands [48–50].

4. Discussion

4.1. Advantages of the Classification Method of Wetlands

Most previous studies have realized the classification of wetlands by extracting many feature variables. However, classification accuracy and efficiency were greatly affected by many feature variables. Therefore, it was crucial to optimize the feature variables according to local conditions before classification. The RF algorithm had greater advantages in determining the optimal subset of feature variables because it could automatically judge the importance of variables and give the dependence among variables. In this paper, the optimal feature variable sets in the YRD were determined utilizing the RF method, which could provide important references for relative investigations of wetland in the Yellow River delta. Then, six classification schemes were designed and tested, and it was found that scheme F had the best classification accuracy. This was because scheme F eliminated the feature variables with a low contribution rate to classification through the RF method, so that the remaining feature variables had low information redundancy, which was conductive to enhance the classification accuracy. The classification accuracy was reduced when all feature variables were utilized to extract wetland information based on the RF method. This was consistent with the results of Song et al. [51]. Scheme C had better classification accuracies than schemes E and D because there was low redundancy between spectral features and the red-edge index. In addition, the red-edge index was a better indicator to reflect the grown condition of vegetation, which was conductive to enhancing the classification accuracy of wetlands [52]. The overall classification accuracy based on the RF method and the optimal feature variable sets was higher than other methods (SVM classification [53], supervised classification [54]), which could provide technical references for related research in the YRD and other regions.

4.2. Causes of Wetland Change Pattern

The wetlands in the YRD showed coastal and riverside distribution characteristics. The reason was that a large area of land extending to the ocean had formed mud flats and shallow waters. In addition, reservoirs, ponds, and salt pans were mostly developed in coastal or riverside regions, with severe salinization that were not conducive to the growth of ordinary crops. To ensure economic income, marine aquaculture reservoirs, ponds, and salt pans are vigorously developed in the region.

During 2015–2021, the new-born and distinction wetlands mainly occurred in the coastal areas. The reasons were that the northern Hekou district and the eastern coast of Kenli district had large areas of shallow waters, mud flats, reservoirs, ponds, and other wetland types, and the coastal areas of the YRD had dramatic alternation of the land-sea boundary. Due to the continuous water and sediment transport of the Yellow River in the northeast of the Kenli district, the delta showed an expansion trend toward the ocean. In recent years, more unused land has been converted to paddy fields, rivers, reservoirs, ponds, and salt pans to improve the regional economy in coastal areas.

5. Conclusions

Based on Sentinel-2 images and RF methods, the optimal feature variable sets for wetland classification in the YRD were determined, and then the spatial distribution of wetlands in 2015 and 2021 were obtained. Finally, the change pattern and driving mechanism of wetlands during 2015–2021 were analyzed based on the gravity center model and geographical detector. The major conclusions were as follows:

(1) Vegetation index and water index have a positive impact on wetland information extraction and classification accuracy. In addition, the red-edge index made greater contributions to enhance classification accuracy.

(2) The Random Forest algorithm could be used to optimize the feature variables, and remove the redundancy among feature variables. Scheme F, based on optimal feature variable sets, had the best classification accuracy of wetlands, which could provide references for the investigation of wetlands in the YRD.
(3) During 2015–2021, a large area of natural wetland in the YRD was transformed into an artificial wetland. The wetlands showed an overall development direction of "northwest–southeast" along the Yellow River.
(4) Wetland changes in the YRD were affected by both natural and human factors. The interaction between FVC and accumulated temperature had the largest explanatory power of the change in the natural wetland area. The interaction between solar radiation and DEM had the largest explanatory power for the change in the artificial wetland area.

In this paper, the study period (2015–2021) was not long enough to reveal the evolutionary process of the wetland in the YRD. In further studies, longer time series remote sensing images would be applied to investigate the spatio-temporal change patterns of wetlands. Moreover, the landscape pattern index should be adopted to analyze the spatial structure characteristics of different types of wetlands.

Author Contributions: Conceptualization, methodology, writing—original draft preparation, C.W. and B.G. Investigation, supervision, project administration, funding acquisition, Y.F., W.Z. and J.J. All authors have read and agreed to the published version of the manuscript.

Funding: This research was funded by the National Natural Science Foundation of China, grant number 42101306; the Natural Science Foundation of Shandong Province, grant number ZR2021MD047, A grant from State Key Laboratory of Resources and Environmental Information System; the Open fund of Key Laboratory of National Geographic Census and Monitoring, MNR grant number 2020NGCM02; the Open Fund of Key Laboratory of Urban Land Resources Monitoring and Simulation, Ministry of Natural Resources, grant number KF-2020-05-001, and the Major Project of High Resolution Earth Observation System of China, grant number GFZX0404130304.

Data Availability Statement: Not applicable.

Conflicts of Interest: The authors declare no conflict of interest.

Abbreviation

Full Name	Abbreviation
Yellow River delta	YRD
Classification and Regression Tree	CART
Support Vector Machine	SVM
Random Forest	RF
Artificial Neural Network	ANN
K-Nearest Neighbors	KNN
Google Earth Engine	GEE
Digital Elevation Model	DEM
Bidirectional Reflectance Distribution Function	BRDF
Principal component analysis	PCA
Gray Level Co-occurrence Matrix	GLCM
Overall Accuracy	OA
Kappa coefficient	Kappa
Producer's Accuracy	PA
User's Accuracy	UA
Land Use/Cover Change	LUCC
Out-Of-Bag	OOB
Geographic Information System	GIS
Remote Sensing	RS
Vegetation Coverage	FVC
Gross Domestic Product	GDP

References

1. Davidson, N.C. How much wetland has the world lost? Longterm and recent trends in global wetland area. *Mar. Freshw. Res.* **2014**, *65*, 934–941. [CrossRef]
2. Escorihuel, M.J.; Quintana, S.P.; Escorihuel, M.J. Comparison of remote sensing and simulated soil moisture datasets in Mediterranean landscapes. *Remote Sens. Environ.* **2016**, *180*, 99–114. [CrossRef]
3. Steven, A.S.; Douglas, A.; Liou, W.S. Accuracy of Landsat-TM and GIS rule-based methods for forest wetland classification in Maine. *Remote Sens. Environ.* **1995**, *53*, 133–144.
4. Ozesmi, S.L.; Marvin, E.B. Satellite remote sensing of wetlands. *Wetl. Ecol. Manag.* **2002**, *10*, 381–402. [CrossRef]
5. Aurélie, D.; Gaëtan, L.; Brigitte, P. Wetland monitoring using classification trees and SPOT-5 seasonal time series. *Remote Sens. Environ.* **2009**, *114*, 552–562.
6. Zhang, C.; Zang, S.Y.; Jin, Z.; Zhang, Y.H. Remote sensing classification for Zhalong Wetlands based on support vector machine. *Wetl. Sci.* **2011**, *9*, 263–269.
7. Abdelgadir, A.A.; Sucharita, G.; James, R.I.; Alan, H.S. Classification of ASAS multiangle and multispectral measurements using artificial neural networks. *Remote Sens. Environ.* **1996**, *57*, 79–87.
8. Khatami, R.; Mountrakis, G.; Stephen, V. A meta-analysis of remote sensing research on supervised pixel-based land-cover image classification processes: General guidelines for practitioners and future research. *Remote Sens. Environ.* **2016**, *177*, 89–100. [CrossRef]
9. Noi, P.T.; Kappas, M. Comparison of Random Forest, k-Nearest Neighbor, and Support Vector Machine Classifiers for Land Cover Classification Using Sentinel-2 Imagery. *Sensors* **2018**, *18*, 18.
10. Dehkordi, A.T.; Zoej, M.J.V.; Ghasemi, H.; Ghaderpour, E.; Hassan, Q.K. A new clustering method to generate training samples for supervised monitoring of long-term water surface dynamics using Landsat data through Google Earth Engine. *Sustainability* **2022**, *14*, 8046. [CrossRef]
11. Gxokwe, S.; Dube, T.; Mazvimavi, D. Leveraging Google Earth Engine platform to characterize and map small seasonal wetlands in the semi-arid environments of South Africa. *Sci. Total Environ.* **2022**, *803*, 150139. [CrossRef] [PubMed]
12. Chi, Y.; Shi, H.H.; Sun, J.K.; Li, J.; Yang, F.; Fu, Z.Y. Spatio-temporal characteristics and main influencing factors of vegetation net primary productivity in the Yellow River Delta in recent 30 years. *Acta Ecol. Sin.* **2018**, *38*, 2683–2697.
13. Zhang, X.L.; Ye, S.Y.; Yin, P.; Chen, J.D. Characters and successions of natural wetland vegetation in Yellow River Delta. *Ecol. Environ. Sci.* **2009**, *18*, 292–298.
14. Talukdar, S.; Singha, P.; Mahato, S.; Liou, Y.A.; Rahman, A. Land-use land-cover classification by machine learning classifiers for satellite observations-A review. *Remote Sens.* **2020**, *12*, 1135. [CrossRef]
15. Abdi, A.M. Land cover and land use classification performance of machine learning algorithms in a boreal landscape using Sentinel-2 data. *GIScience Remote Sens.* **2020**, *57*, 1–20. [CrossRef]
16. Wang, M.; Qi, S.; Zhang, X. Wetland loss and degradation in the Yellow River Delta, Shandong Province of China. *Environ. Earth Sci.* **2012**, *67*, 185–188. [CrossRef]
17. Liu, G.L.; Zhang, L.C.; Zhang, Q.; Musyimi, Z.; Jiang, Q.H. Spatio–Temporal Dynamics of Wetland Landscape Pat-terns Based on Remote Sensing in Yellow River Delta, China. *Wetlands* **2014**, *34*, 787–801. [CrossRef]
18. Zhou, K. Wetland landscape pattern evolution and prediction in the Yellow River Delta. *Appl. Water Science.* **2022**, *12*, 190. [CrossRef]
19. Chen, Z.R.; Zhang, X.X.; Hu, H.H.; Niu, Y.Y.; Ye, J.F.; Zhang, Q.; Liu, B.; Zhao, L.N.; Lu, S.; Lu, L.M.; et al. Plant geography in China: History, progress and prospect. *Acta Geogr. Sin.* **2022**, *77*, 120–132.
20. Guo, B.; Yang, F.; Fan, J.F.; Lu, Y.F. The changes of spatiotemporal pattern of rocky desertification and its dominant driving factors in typical Karst mountainous areas under the background of global change. *Remote Sens.* **2022**, *14*, 2351. [CrossRef]
21. Zhang, L.; Gong, Z.N.; Wang, Q.W.; Jin, D.D.; Wang, X. Wetland mapping of Yellow River Delta wetlands based on multi-feature optimization of Sentinel-2 images. *J. Remote Sens.* **2019**, *23*, 313–326.
22. Ortega, P.M.; Montero, L.G.G.; Sibelet, N. Temporal patterns in illumination conditions and its effect on vegetation indices using Landsat on Google Earth Engine. *Remote Sens.* **2022**, *12*, 211. [CrossRef]
23. Office of International Standards and Legal Affairs. UNESCO. Convention on wetlands pf international importance especially as waterfowl habitat. In Proceedings of the Second Conference of the Parties, Groningen, The Netherlands, 7–12 May 1984.
24. Huang, K.; Shi, D.Z.S.; Deng, C.L.; Du, K. Response relationship between ecosystem and runoff into the sea in the Yellow River. *Yellow River* **2012**, *34*, 66–69.
25. Mu, X.J.; Liu, X.T.; Yan, B.X.; Cui, B.S. Classification system of coastal wetlands in China. *Wetl. Sci.* **2015**, *13*, 19–26.
26. Liu, G.Y.; Huang, Y.; Cao, Y.; Zeng, Z.Y.; Zhao, E.M. Research on extraction of image texture feature based on gray co-occurrence matrix. *Wind. Sci. Technol.* **2021**, *12*, 61–64.
27. Li, H.K.; Wang, L.J.; Xiao, S.S. Random forest classification of land use in hilly and mountaineous areas of southern China using multi-source remote sensing data. *Trans. Chin. Soc. Agric. Eng.* **2021**, *37*, 244–251.
28. Na, X.D.; Zhang, S.Q.; Kong, B.; Yu, H.; Liu, C.Y. The extraction of freshwater marsh wetland information based on Decision Tree Algorithm- A case study in the northeast of the Sanjiang Plain. *Remote Sens. Technol. Appl.* **2008**, *23*, 265–372.
29. Kumari, N.; Srivastava, A.; Dumka, U.C. A long-term spatiotemporal analysis of vegetation greenness over the Himalayan Region using Google Earth Engine. *Climate* **2021**, *9*, 109. [CrossRef]

30. Du, Z.F. *Multivariate Statistical Analysis*; Tsinghua University Press: Beijing, China, 2016.
31. Deng, N.D.; Li, Y.X.; Cui, Y.Y.; Shi, H.; Guo, Y.L. Landslide susceptibility assessment based on hybrid model of machine learning. *Sci. Technol. Eng.* **2022**, *22*, 5539–5547.
32. Fabian, B.; Kai, Z. Thermal influences on groundwater in urban environments—A multivariate statistical analysis of the subsurface heat island effect in Munich. *Sci. Total Environ.* **2022**, *810*, 152193.
33. Haralick, R.M. Statistical and structural approaches to texture. *Proc. IEEE* **1979**, *67*, 786–804. [CrossRef]
34. Dong, K.; Yu, Z.; Kerfahi, D.; Sang, S.L.; Li, N.; Yang, T.; Adams, J.M. Soil microbial co-occurrence networks become less connected with soil development in a high Arctic glacier foreland succession. *Sci. Total Environ.* **2022**, *813*, 152565. [CrossRef] [PubMed]
35. Belwalkar, A.; Pobleta, T.; Longmire, A.; Hornero, A.; Hernandez, R.C.; Tejada, P.J.Z. Evaluation of SIF retrievals from narrow-band and sub-nanometer airborne hyperspectral imagers flown in tandem: Modelling and validation in the context of plant phenotyping. *Remote Sens. Environ.* **2022**, *273*, 112926. [CrossRef]
36. Wang, S.J. Study on feature extraction and semi-supervised classification for hyperspectral remote sensing imagery. *Nanjing Norm. Univ.* **2016**. [CrossRef]
37. Iverson, L.R.; Prasad, A.M.; Matthews, S.N. Estimating potential habitat for 134 eastern US tree species under six climate scenarios. *For. Ecol. Manag.* **2008**, *254*, 390–406. [CrossRef]
38. Breiman, L. Random forest. *Mach. Learn.* **2001**, *45*, 5–32. [CrossRef]
39. Virro, H.; Kmoch, A.; Vainu, M.; Unemaa, E. Random forest-based modeling of stream nutrients at national level in a data-scarce region. *Sci. Total Environ.* **2022**, *840*, 156613. [CrossRef]
40. Solmaz, F.; Mohammad, K.F.; Li, H.J.; Asim, B. Surface biophysical features fusion in remote sensing for improving land crop/cover classification accuracy. *Sci. Total Environ.* **2022**, *838*, 156520.
41. Wang, L.J.; Kong, Y.R.; Xu, Y.; Liang, L.; Wang, S.G. Classification of land use in farming areas based on feature optimization random forest algorithm. *Trans. Chin. Soc. Agric. Eng.* **2020**, *36*, 244–250.
42. Gao, Z.P.; Guo, H.M.; Li, S.Y.; Wang, J.; Ye, H.L.; Han, S.B.; Cao, W.G. Remote sensing of wetland evolution in predicting shallow groundwater arsenic distribution in two typical inland basins. *Sci. Total Environ.* **2022**, *806*, 150496. [CrossRef]
43. Jiang, S.; Meng, J.J.; Zhu, L.K.; Cheng, H.R. Spatial-temporal pattern of land use conflict in China and its multilevel driving mechanisms. *Sci. Total Environ.* **2021**, *801*, 149697. [CrossRef]
44. Zan, C.J.; Liu, T.; Huang, Y.; Bao, A.M.; Yan, Y.Y.; Ling, Y.N.; Wang, Z.; Duan, Y.C. Spatial and temporal variation and driving factors of wetland in the Amu Darya River Delta, Central Asia. *Ecol. Indic.* **2022**, *139*, 108898. [CrossRef]
45. Zhang, Y.R.; Wen, X.H.; Luo, S.Q.; Li, M.S. Study on the relationship between vegetation cover change and climate factors in Zoige wetland in recent 20 year. *Plateau Meteorol.* **2022**, *41*, 317–327.
46. Jia, J.J.; Wang, Y.F.; Lu, Y.; Sun, K.; Lu, S.D.; Gao, Y. Driving mechanisms of gross primary productivity geographical patterns for Qinghai–Tibet Plateau lake systems. *Sci. Total Environ.* **2021**, *791*, 148286. [CrossRef] [PubMed]
47. Venkatesh, K.; John, R.; Chen, J.Q.; Xiao, J.F.; Amirkhiz, R.G.; Giannico, V.; Kussainova, M. Optimal ranges of social-environmental drivers and their impacts on vegetation dynamics in Kazakhstan. *Sci. Total Environ.* **2022**, *847*, 157562. [CrossRef]
48. Yan, J.N.; Liu, J.W.; Wang, L.Z.; Liang, D.; Cao, Q.C.; Zhang, W.F.; Jiang, P. Land-cover classification with time-series remote sensing images by complete extraction of multiscale timing dependence. *IEEE J. Sel. Top. Appl. Earth Obs. Remote Sens.* **2022**, *15*, 1953–1967. [CrossRef]
49. Guo, B.; Wei, C.X.; Yu, Y.; Liu, Y.F.; Li, J.L.; Meng, C.; Cai, Y.M. The dominant influencing factors of desertification changes in the source region of Yellow River: Climate change or human activity? *Sci. Total Environ.* **2022**, *813*, 152512. [CrossRef]
50. Chen, S.T.; Guo, B.; Zhang, R.; Zang, W.Q.; Wei, C.X.; Wu, H.W.; Yang, X.; Zhen, X.Y.; Li, X.; Zhang, D.F.; et al. Quantitatively determine the dominant driving factors of the spatial-temporal changes of vegetation NPP in the Hengduan Mountain area during 2000–2015. *J. Mt. Sci.* **2021**, *18*, 427–445. [CrossRef]
51. Song, H.R.; Su, G.H.; Sun, J.H.; Lin, W.R. Landscape changes of the Yancheng wetland in the past 20 years: Evidence from Random Forest. *Mar. Geol. Front.* **2021**, *37*, 75–82.
52. Pu, Y.H.; Zhang, D.; Xu, D.D.; Luan, Z.Q. Evaluation of red edge of Sentinel-2A in vegetation classification of lakeside zone. *For. Resour. Manag.* **2021**, *2*, 131–139.
53. Wei, Y.Q.; Wang, W.W.; Tang, X.J.; Li, H.; Hu, H.W.; Wang, X.F. Classification of alpine grasslands in cold and high altitudes based on multispectral Landsat-8 images: A case study in Sanjiangyuan National Park, China. *Remote Sens.* **2022**, *14*, 3714. [CrossRef]
54. Gao, R.; Wang, Z.Y.; Zhou, X.D.; Liu, R. Monitoring and analysis of wetland change dynamics in the Yellow River Delta using multi-temporal remote sensing. *Surv. Mapp. Bull.* **2021**, *4*, 22–27.